International Journal of Heat and Mass Transfer 67 (2013) 311–325

Contents lists available at ScienceDirect

International Journal of Heat and Mass Transfer

journal homepage: www.elsevier.com/locate/ijhmt

Numerical simulation of a crossflow moving porous bed using a thermal non-equilibrium model

Ana C. Pivem, Marcelo J.S. de Lemos *

Departamento de Energia – IEME, Instituto Tecnológico de Aeronáutica – ITA, 12228-900 São José dos Campos, SP, Brazil

ARTICLE INFO

Article history:
Received 19 March 2013
Received in revised form 27 July 2013
Accepted 28 July 2013

Keywords:
Crossflow
Moving bed
Porous media
Heat transfer

ABSTRACT

This study investigates the influence of physical properties on heat transfer between solid and fluid phases in a cross flow moving porous bed, in which the fluid moves with longitudinal and transversal components with respect to the permeable bed. For simulating flow and heat transfer, a two-energy equation model is applied in addition to a mechanical model. Transport equations are discretized using the control-volume method and the system of algebraic equations is relaxed via the SIMPLE algorithm. The effects of flow properties, such as Reynolds number, solid-to-fluid velocity ratio, permeability and porosity, as well as the effects of thermal properties, namely solid-to-fluid thermal capacity and solid-to-fluid thermal conductivity ratio, are analyzed. The numerical results show that the Reynolds number affects strongly the flow behavior and for high values of the solid-to-fluid velocity ratio, solid-to-fluid thermal capacity ratio and solid-to-fluid thermal conductivity ratio, there is a decrease in temperature gradients everywhere in the domain and the fluid temperature reaches higher values mainly in the symmetry region of the channel.

1. Introduction

Among design concepts for moving bed equipment, the cross flow configuration has been used in many engineering equipment. Moving bed technology has wide application on devices and processes such as heat exchangers, evaporators, inter-coolers, pre-heaters, condensers, drying of grains and seeds, among others.

The crossflow configuration can happen among fluids or between fluid and solid, as in the case of moving bed, where in this configuration, the fluid phase is in perpendicular direction with that of the solid phase.

With the respect of the crossflow moving bed heat exchangers, Zhao et al. [1] simulate a moving granular bed for combined hot gas desulfurization with dust removal, Lozano et al. [2] shows the modeling of a new crossflow moving bed heat exchanger filter and Almendros-Ibáñez et al. [3] presents a theoretical study of the energetic performance of a moving bed heat exchanger, which consists of a flow and solid particles moving downwards, which recovered heat from a gas flow percolating a solid phase in crossflow.

In accompanying papers, co-current [4] as well as counter flows [5] in moving porous beds were investigated using a two-equation approach for handling thermal-non-equilibrium [6]. In [4,5] a model for treating the movement of the solid phase was employed [7]. Therein, only aligned flow cases were investigated, or say, the movement of the solid porous matrix was aligned with that of the working fluid. For co-current configurations, both phases had speed with the same sign whereas in counter-flow configurations the fluid and solid moved on opposing directions to each other.

The objective of the present contribution is to extend the previous analysis of parallel [4] and counter flows [5], which used the energy model of [6,7], to investigate now cross-flow configurations. Here, the fluid phase flows in a direction not aligned with the steadily moving solid matrix. By that, a number of engineering flows of practical relevance can be evaluated such as flow in downdraft crossflow gasifiers and in equipment for advanced materials production. As such, the results to be shown below may benefit the design and analysis of engineering equipment used in gasification processes and for manufacturing advanced materials.

1.1. Macroscopic model for flow equations

The equations to follow are available in the open literature and for that their derivation are not repeated here [8]. Further, before transport equations for the moving bed cases are presented, the mathematical model for a fixed bed are shown for the sake of completeness.

1.2. Fixed bed

A macroscopic form of the governing equations is obtained by taking the volumetric average of the entire equation set. In this development, the porous medium is considered to be rigid, fixed

* Corresponding author. Tel.: +55 12 3947 5860; fax: +55 12 3947 5842.
E-mail address: delemos@ita.br (M.J.S. de Lemos).

0017-9310/$ - see front matter © 2013 Elsevier Ltd. All rights reserved.
http://dx.doi.org/10.1016/j.ijheatmasstransfer.2013.07.087

Nomenclature

A_i	interfacial area	$\langle T_f \rangle$	fluid temperature
a_i	interfacial area per unit volume	$\langle T_s \rangle$	solid temperature
c_F	Forchheimer coefficient	$\mathbf{u}$	microscopic velocity vector
c_p	specific heat	$\langle \mathbf{u} \rangle^i$	intrinsic (fluid) average of $\mathbf{u}$
D	particle diameter	$\mathbf{u}_D$	Darcy velocity vector, $\mathbf{u}_D = \phi \langle \mathbf{u} \rangle^i$
$\mathbf{D}$	deformation rate tensor, $\mathbf{D} = [\nabla \mathbf{u} + (\nabla \mathbf{u})^T]/2$	$u_D \hat{i}$	Darcy velocity component in the direction x
H	distance between channel walls	$\mathbf{u}_{rel}$	relative velocity based on total volume
h_i	interfacial heat transfer coefficient	$v_D \hat{j}$	Darcy velocity component in the direction y
K	permeability	*Greek*	
$\mathbf{K}_{eff}$	effective thermal dispersion tensor	γ	phase identifier
k_s/k_f	thermal conductivity ratio	μ	fluid dynamic viscosity
L	channel length	ρ	density
p	thermodynamic pressure	ϕ	porosity
$\langle p \rangle^i$	intrinsic (fluid) average of pressure p	*Subscript*	
Re	Reynolds number, $Re_H = \rho u_{D_{in}} 2H/\mu$, $Re_D = \rho \lvert \mathbf{u}_{rel} \rvert D/\mu$	s,f	s = solid, f = fluid

and saturated by an incompressible fluid. As mentioned, derivation of this equation set is already available in the literature [8] so that details need not to be repeated here. Nevertheless, for the sake of completeness, the final laminar incompressible form of the equations is here presented:

Continuity:

$$\nabla \cdot \mathbf{u}_D = 0 \tag{1}$$

Momentum:

$$\rho \left[\frac{\partial \mathbf{u}_D}{\partial t} + \nabla \cdot \left(\frac{\mathbf{u}_D \mathbf{u}_D}{\phi} \right) \right] = -\nabla \left(\phi \langle \bar{p} \rangle^i \right) + \mu \nabla^2 \mathbf{u}_D - \left[\frac{\mu \phi}{K} \mathbf{u}_D + \frac{c_F \phi \rho |\mathbf{u}_D| \mathbf{u}_D}{\sqrt{K}} \right], \tag{2}$$

where the last two terms in Eq. (2) represent the Darcy and Forchheimer contributions, respectively. The quantity $\phi = \Delta V_f / \Delta V$ in Eq. (2) that represents the volume ratio occupied by the fluid, here named *porosity*, is sometimes referred to in the literature as *voidage*.

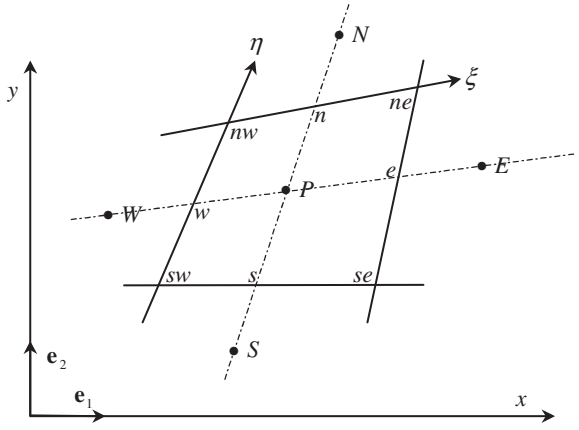

Fig. 2. Control volume and notation.

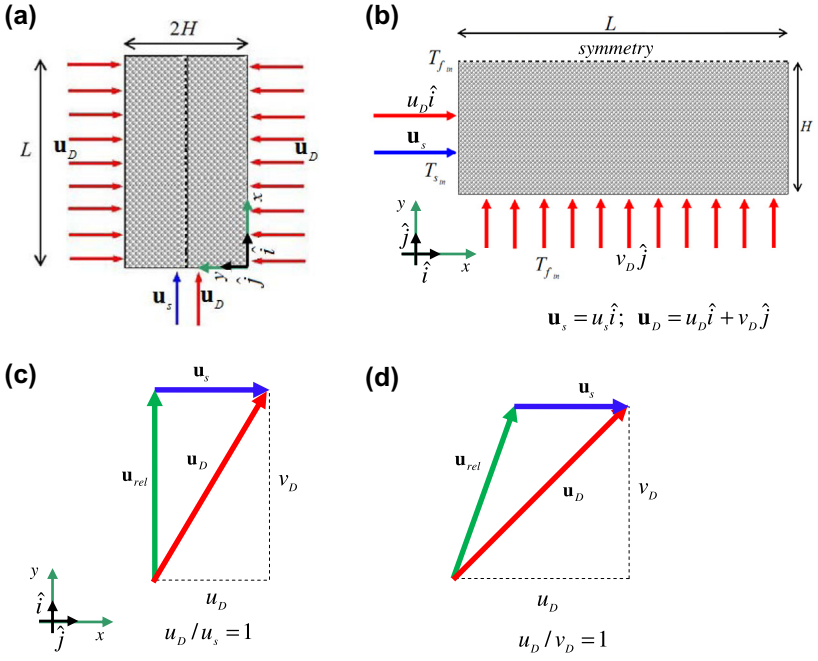

Fig. 1. Porous bed reactor with a moving solid matrix: (a,b) crossflow with fluid moving southwest to northeast (geometry turned 90 degrees counterclockwise); (c) flow configurations with $u_D/u_s = 1$; (d) flow configurations with $u_D/v_D = 1$.

Table 1
Cases and parameters used.

Cases investigated	Dimensional					Non-dimensional					
	u_D [m/s]	u_s [m/s]	v_D [m/s]	u_{rel} [m/s]	K[m^2]	Re_D	u_s/v_D	Da	ϕ	$(\rho c_p)_s/(\rho c_p)_f$	k_s/k_f
Effect of Re_D	1.416E-02	1.416E-02	2.833E-02	2.833E-02	2.025E-05	1.00E01	5.0E-01	3.37E-03	0.9	1.5E00	2.5E01
	7.083E-02	7.083E-02	1.416E-02	1.416E-02		5.00E01					
	1.416E-01	1.416E-01	2.833E-01	2.833E-01		1.00E02					
Effect of u_S/u_D	0.000E00	0.00E00	2.833E-01	2.833E-01	2.025E-05	1.00E02	0.0E00	3.37E-03	0.9	1.5E00	2.5E01
	7.083E-02	7.083E-02					2.5E-01				
	1.416E-01	1.416E-01					5.0E-01				
	2.124E-01	2.124E-01					7.5E-01				
	2.691E-01	2.691E-01					9.5E-01				
Effect of Da	1.062E-01	1.062E-01	2.125E-01	2.125E-01	9.000E-06	5.00E01	5.0E-01	1.50E-03	0.9	1.5E00	2.5E01
					3.600E-05	1.00E02		5.99E-03			
					5.620E-05	1.25E02		1.00E-02			
Effect of ϕ	1.062E-01	1.062E-01	2.125E-01	2.125E-01	1.111E-07	7.5E01	5.0E-01	1.85E-05	0.4	1.5E00	2.5E01
					5.620E-07			9.36E-05	0.6		
					4.000E-06			6.66E-04	0.8		
Effect of $(\rho c_p)_s/(\rho c_p)_f$	1.062E-01	1.062E-01	2.125E-01	2.125E-01	2.025E-05	7.5E01	5.0E-01	3.37E-03	0.9	2.5E-01	2.5E01
										5.0E-01	
										1.0E00	
										1.0E01	
Effect of $k_s/k_f, u_S/u_D = 0$	0.000E00	0.000E00	2.125E-01	2.125E-01	2.025E-05	7.5E01	0.0E00	3.37E-03	0.9	1.5E00	1.0E00
											1.0E01
											1.0E02
											1.0E03
Effect of k_s/k_f, $u_S/u_D = 0.1$	2.125E-02	2.125E-2	2.125E-01	2.125E-01	2.025E-05	7.5E01	1.0E-01	3.37E-03	0.9	1.5E00	1.0E00
											1.0E01
											1.0E02
											1.0E03
Effect of $k_s/k_f, u_S/u_D = 0.4$	8.500E-2	8.500E-2	2.125E-01	1.275E-01	2.025E-05	7.5E01	4.0E-01	3.37E-03	0.9	1.5E00	1.0E00
											1.0E01
											1.0E02
											1.0E03

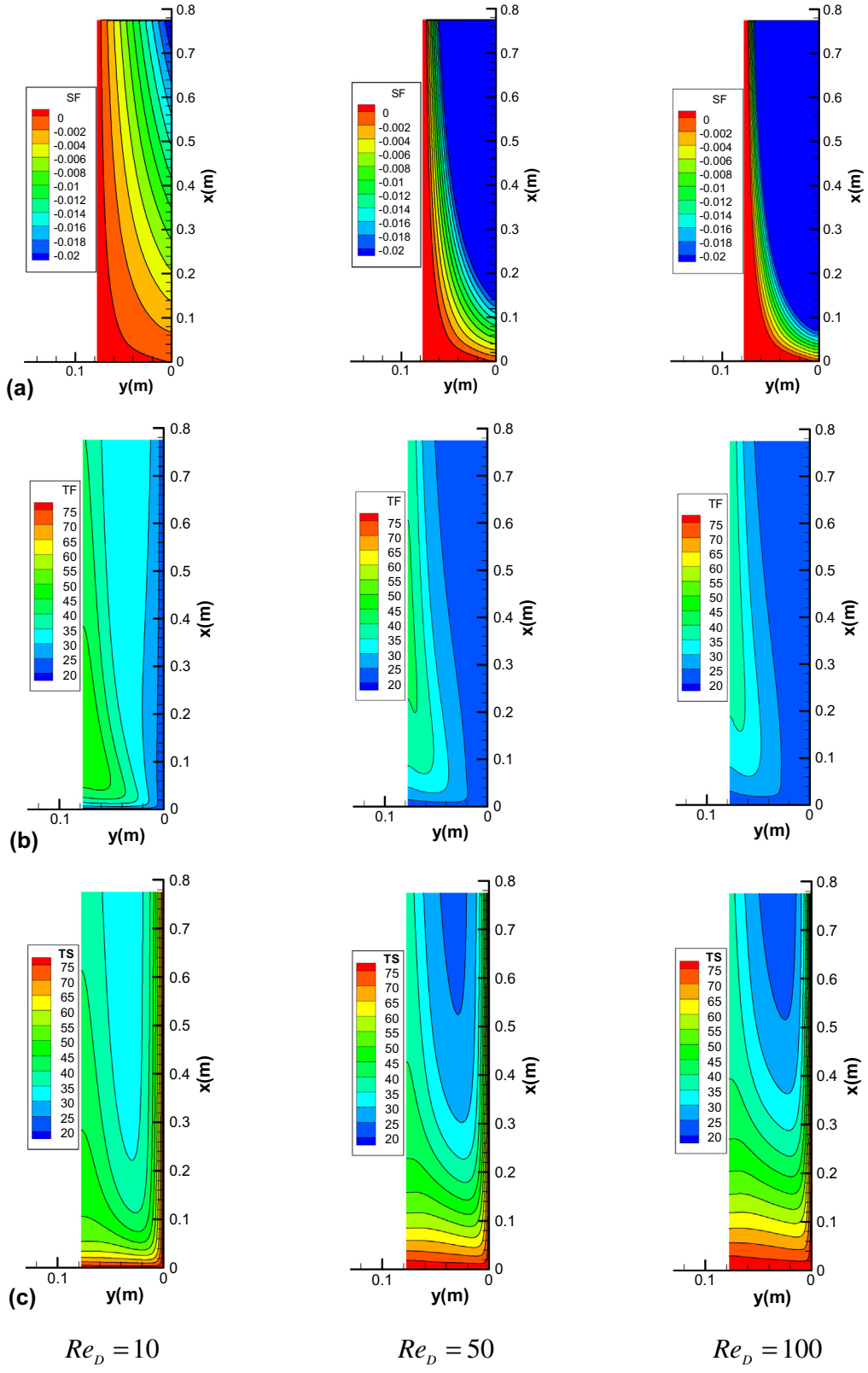

Fig. 3. Dimensional temperatures as a function of Re_D; $u_s/V_D = 0.5$, $\phi = 0.9$, $k_s/k_f = 25$, $Da = 3.37 \times 10^{-3}$, $(\rho c_p)_s/(\rho c_p)_c = 1.5$: (a) streamlines, (b) fluid temperature, (c) solid temperature.

1.3. Moving bed

When the solid phase moves in relation to the fluid phase, only cases where the porous matrix speed is kept constant will be considered here, or say, we consider a moving bed that crosses a fixed control volume in addition to a flowing fluid, which is not necessarily moving with a velocity aligned with the solid phase velocity. For the sake of clarity, the steps below show some basic definitions prior to presenting a proposal for a set of transport equations for analyzing such systems.

A general form for a volume-average of any property φ, distributed within a phase γ that occupy volume ΔV_γ, can be written as [9,10],

$$\langle\varphi\rangle^\gamma = \frac{1}{\Delta V_\gamma}\int_{\Delta V_\gamma} \varphi\, dV_\gamma \tag{3}$$

In the general case, the volume ratio occupied by phase γ will be $\varphi^\gamma = \Delta V_\gamma/\Delta V$.

If there are two phases, a solid $\gamma = s$ and a fluid phase $\gamma = f$, volume average can be established on both regions. Also,

$$\phi^s = \Delta V_s/\Delta V = 1 - \Delta V_f/\Delta V = 1 - \phi^f \tag{4}$$

and for simplicity of notation one can drop the superscript "f" to get

$$\phi^s = 1 - \phi \tag{5}$$

As such, calling the instantaneous local velocities for the solid and fluid phases, $\mathbf{u}_s$ and $\mathbf{u}$, respectively, one can obtain the average for the solid velocity, within the solid phase, as follows,

$$\langle\mathbf{u}\rangle^s = \frac{1}{\Delta V_s}\int_{\Delta V_s} \mathbf{u}_s\, dV_s \tag{6}$$

which, in turn, can be related to an average velocity referent to the entire REV as,

$$\mathbf{u}_S = \overbrace{\frac{\Delta V_s}{\Delta V}}^{(1-\phi)}\underbrace{\frac{1}{\Delta V_s}\int_{\Delta V_s} \mathbf{u}_s\, dV_s}_{\langle\mathbf{u}\rangle^s} \tag{7}$$

A further approximation herein is that the porous bed is kept rigid and moves with a steady average velocity $\mathbf{u}_s$.

Both velocities can then be written as,

$$\mathbf{u}_D = \phi\langle\mathbf{u}\rangle^i \quad \text{and} \quad \mathbf{u}_s = (1-\phi)\langle\mathbf{u}\rangle^s = const \tag{8}$$

A relative velocity is then defined as,

$$\mathbf{u}_{rel} = \mathbf{u}_D - \mathbf{u}_S \tag{9}$$

Here, for simplicity, we assume that the relative macroscopic movement between the two phases is governed by Eq. (9) instead of $\langle\mathbf{u}\rangle^i - \langle\mathbf{u}\rangle^s$. Or say, we assume the relative velocity to be based on the total volume instead of the phase volume. With this in mind, the momentum equation reads,

$$\rho\left[\frac{\partial\mathbf{u}_D}{\partial t} + \nabla\cdot\left(\frac{\mathbf{u}_D\mathbf{u}_D}{\phi}\right)\right] = -\nabla(\phi\langle\bar{p}\rangle^i) + \mu\nabla^2\mathbf{u}_D - \underbrace{\left[\frac{\mu\phi}{K}\mathbf{u}_{rel} + \frac{c_F\phi\rho|\mathbf{u}_{rel}|\mathbf{u}_{rel}}{\sqrt{K}}\right]}_{relative\ drag}, \tag{10}$$

1.4. Two-energy equation model

In a similar manner as above, macroscopic equations for heat transport in porous media are obtained by applying the volume averaging to local equations. Here, the mathematical model used to describe the heat transfer between the solid and fluid phases is based on the so-called two-energy equations model, which can be written as:

$$\{(\rho c_p)_f\phi\}\frac{\partial\langle T_f\rangle^i}{\partial t} + (\rho c_p)_f\nabla\cdot(\mathbf{u}_D\langle T_f\rangle^i) = \nabla\cdot\{\mathbf{K}_{eff,f}\cdot\nabla\langle T_f\rangle^i\} + h_i a_i(\langle T_s\rangle^i - \langle T_f\rangle^i) \tag{11}$$

$$\{(1-\phi)(\rho c_p)_s\}\frac{\partial\langle T_s\rangle^i}{\partial t} + (\rho c_p)_s\nabla\cdot(\mathbf{u}_S\langle T_s\rangle^i) = \nabla\cdot\{\mathbf{K}_{eff,s}\cdot\nabla\langle T_s\rangle^i\} - h_i a_i(\langle T_s\rangle^i - \langle T_f\rangle^i) \tag{12}$$

where, $\mathbf{K}_{eff,f}$ and $\mathbf{K}_{eff,s}$ are the effective conductivity tensors for fluid and solid, respectively, given by:

$$\mathbf{K}_{eff,f} = [\phi k_f]\mathbf{I} + \mathbf{K}_{f,s} + \mathbf{K}_{disp} \tag{13}$$

$$\mathbf{K}_{eff,s} = [(1-\phi)k_s]\mathbf{I} + \mathbf{K}_{s,f} \tag{14}$$

In the above equations $\mathbf{I}$ is the unit tensor and $\mathbf{K}_{disp}$, $\mathbf{K}_{f,s}$ and $\mathbf{K}_{s,f}$ are coefficients defined such that,

$$\text{Thermal dispersion}: -(\rho c_p)_f(\phi\langle{}^i\mathbf{u}^i T_f\rangle^i) = \mathbf{K}_{disp}\cdot\nabla\langle\mathbf{T}_f\rangle^i \tag{15}$$

$$\text{Local conduction}: \begin{cases} \nabla\cdot\left[\frac{1}{\Delta V}\int_{A_i}\mathbf{n}_i k_f T_f\, dA\right] = \mathbf{K}_{f,s}\cdot\nabla\langle T_s\rangle^i \\ -\nabla\cdot\left[\frac{1}{\Delta V}\int_{A_i}\mathbf{n}_i k_s T_s\, dA\right] = \mathbf{K}_{s,f}\cdot\nabla\langle T_f\rangle^i \end{cases} \tag{16}$$

where $\mathbf{n}_i$ in (16) is the unit vector pointing towards the solid phase. In this work, for simplicity, one assumes that the overall thermal resistance between the two phases is controlled by the interfacial film coefficient rather than by the thermal resistance within each phase. As such, the local conduction coefficients $\mathbf{K}_{f,s}$, $\mathbf{K}_{s,f}$ are here neglected for the sake of simplicity. Additional information on the models in Eqs. (13) and (14) can be found in [11].

1.5. Interfacial heat transfer coefficient

The heat transferred between the two phases was modeled by an interstitial heat transfer coefficient, h_i, present in Eqs. (11) and (12) such that,

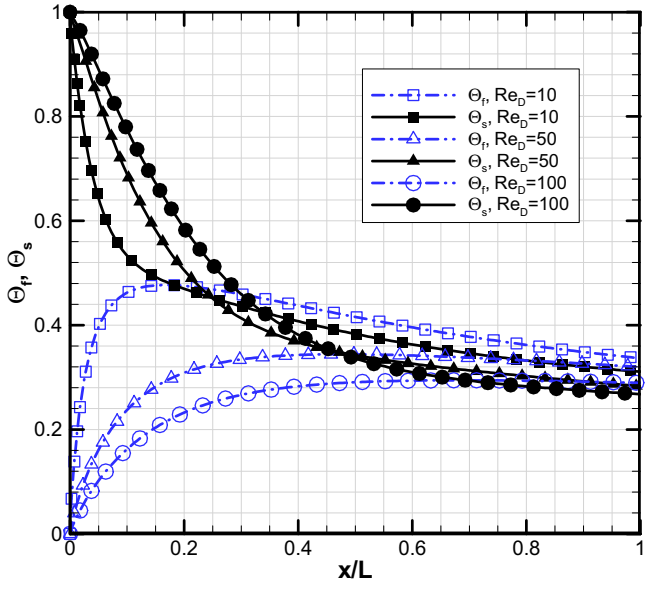

Fig. 4. Non-dimensional temperatures along the symmetry line $y = H$ as a function of Re_D; $u_s/v_D = 0.5$; $k_s/k_f = 25$; $Da = 3.37\times10^{-3}$; $\phi = 0.9$; $(\rho c_p)_s/(\rho c_p)_f = 1.5$.

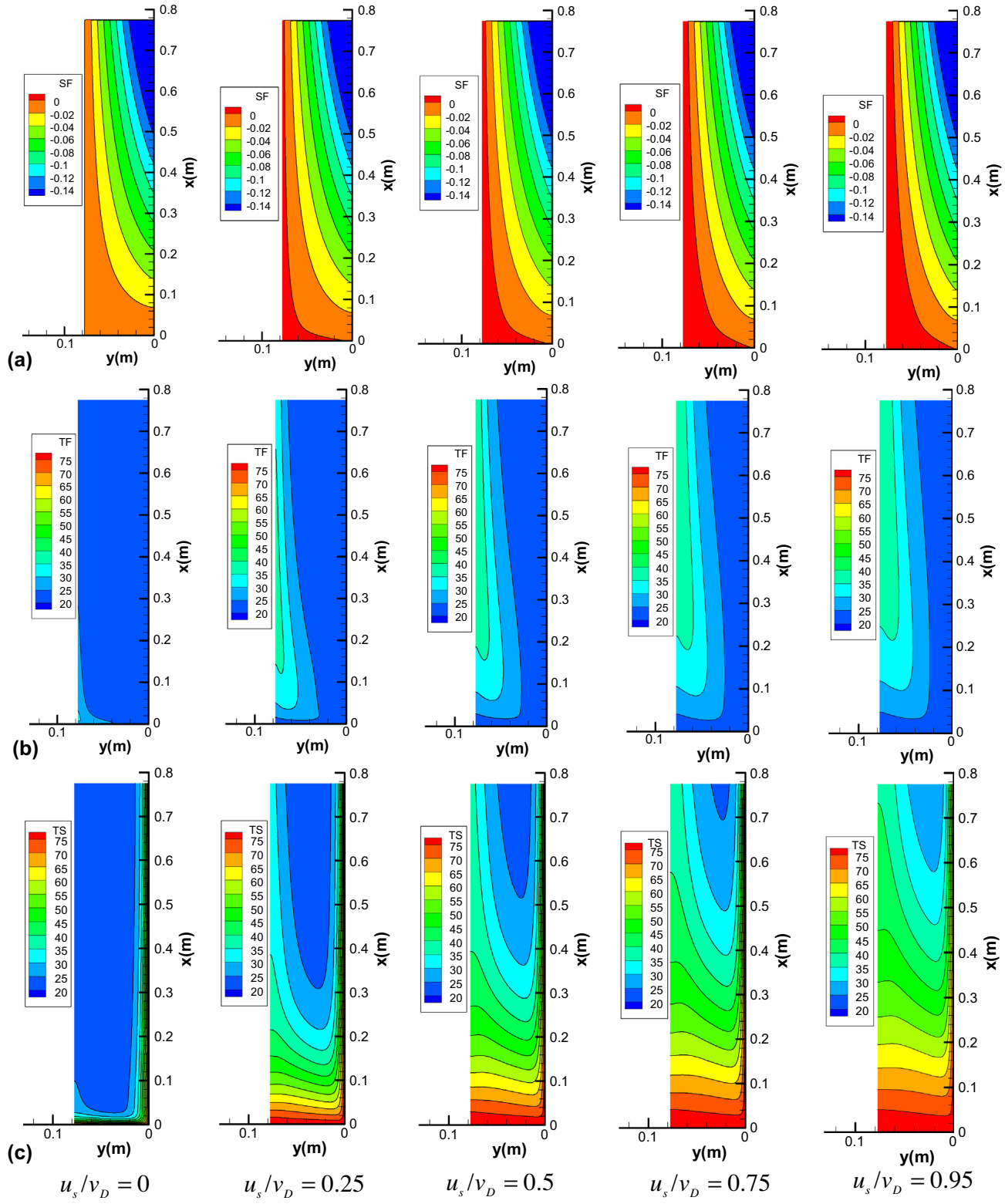

Fig. 5. Dimensional temperatures as a function of u_s/V_D, $k_s/k_f = 25$, $\phi = 0.9$, $Da = 3.37 \times 10^{-3}$, $Re_D = 100$, $(\rho c_p)_s/(\rho c_p)_f = 1.5$: (a) streamlines, (b) fluid temperature, (c) solid temperature.

$$h_i a_i(\langle T_s\rangle^i - \langle T_f\rangle^i) = \frac{1}{\nabla V}\int_{A_i} \mathbf{n}_i \cdot k_f \nabla T_f \, dA = \frac{1}{\Delta V}\int_{A_i} \mathbf{n}_i \cdot k_s \nabla T_s \, dA \tag{17}$$

where A_i is the interfacial area between the two phases and a_i is the interfacial area per unit volume or $a_i = A_i/\nabla V$. Wakao et al. [12] obtained a heuristic correlation for a closely packed bed of particle diameter D and compared their results with experimental

data. This correlation for the interfacial heat transfer coefficient is given by,

$$\frac{h_i D}{k_f} = 2 + 1.1 Re_D^{0.6} Pr^{1/3}, \quad \text{for } \phi > 0.9 \tag{18}$$

Further, a numerical correlation for the interfacial convective heat transfer coefficient was proposed by Kuwahara et al. [13] for a laminar flow as,

$$\frac{h_i D}{k_f} = \left(1 + \frac{4(1-\phi)}{\phi}\right) + \frac{1}{2}(1-\phi)^{1/2} Re_D Pr^{1/3}, \quad \text{valid for } 0.2 < \phi < 0.9 \tag{19}$$

Results in Eq. (19) depend on the porosity and are valid for packed beds of particle diameter D. In addition, Saito and de Lemos [6] also obtained the interfacial heat transfer coefficient for laminar flows through an infinite square rod array using the same methodology as Kuwahara et al. [13].

The interstitial heat transfer coefficient h_i is here calculated by Eq. (19) for laminar flow. However, since the relative movement between phases is seen as the promoter of convective heat transport from the fluid to the solid, or vice-versa, a relative Reynolds number defined as,

$$Re_D = \frac{\rho |\mathbf{u}_{rel}| D}{\mu} \tag{20}$$

is used in correlation Eq. (19) instead of using the absolute velocity of the fluid phase. It is important to emphasize that Re_D is a scalar based on the modulus or magnitude of the relative velocity $|\mathbf{u}_{rel}|$ and, as such, its value depends on both the solid and the fluid velocity and the relative motion between phases, regardless if both currents co-flow, are opposite or perpendicular to each other. Accordingly, when the solid phase velocity approaches that of the fluid, the only mechanism for transferring heat between phases is conduction.

1.6. Geometry, boundary conditions and numerical method

The problem under investigation is a laminar flow through a channel completely filled with a moving layer of a porous material. Fig. 1(a) shows a porous reactor model in which both the porous matrix and fluid enter at that west face located at $x = 0$ (the figure is rotated 90 degrees counterclockwise). In addition to injecting mass at $x = 0$, mass flow enters the model reactor uniformly along the y-direction. As such, a symmetry line can be identified at $y = H$ leading to a computational domain shown Fig. 1(b), which has length and height given by L and H, respectively. Further, Fig. 1 shows two possible crossflow configurations, the first one keeping the ratio $u_D/u_S = 1$ (Fig. 1c) and another maintaining $u_D/v_D = 1$ (Fig. 1(d). Both configurations are considered to be of crossflow type but here only the case shown in Fig. 1(c) is investigated, *i.e.*, simulations to follow used $u_D/u_S = 1$. In addition, in all runs the porous matrix moves with constant positive velocity $\mathbf{u}_s$ and with the same value of the fluid velocity component in x-direction, $u_D\hat{i}$. In the perpendicular y-direction, the fluid velocity component is given by $v_D\hat{j}$ where $v_D\hat{j} > u_D\hat{i}$ in all simulations.

Boundary conditions types are given by:

$$\text{On symmetry, } q_w = 0 \tag{21}$$

On the west face:

$$\mathbf{u}_s = \mathbf{u}_{s_{in}}, \quad u_D\hat{i} = u_{D_{in}}, \langle T_s \rangle^i = T_{s_{in}}, \quad \langle T_f \rangle^i = T_{f_{in}} \tag{22}$$

On south face:

$$v_D\hat{j} = v_{D_{in}}, \quad \langle T_f \rangle^i = T_{f_{in}}, \quad \langle T_s \rangle^i = T_{s_{in}} \tag{23}$$

where $\mathbf{u}_s = u_s\hat{i}, \mathbf{u}_D = u_D\hat{i} + v_D\hat{j}$. (24)

Regardless of the run, in all simulations the inlet fluid and solid temperatures were $T_{f_{in}} = 20$ °C and $T_{s_{in}} = 80$ °C, respectively. Before proceeding, a word about the boundary condition for the solid temperature along the south face in Fig. 1(b), $\langle T_s \rangle^i = T_{s_{in}}$ at $y = 0$, seems important. In fact, any temperature profile could have been specified at that surface that corresponds to the lateral walls of the model reactor presented in Fig. 1(a). For a perfectly insulated vessel, the condition $\partial \langle T_s \rangle^i / \partial y = 0$ could have been applied. For the sake of simplicity, the same temperature at the inlet on the east, $T_{s_{in}}$, was chosen. For a more realistic simulation, however, a different value can be applied and the type of boundary condition used poses no difficulty in the solution procedure here adopted.

The numerical method used to discretize the flow and energy equations was the control volume approach. The SIMPLE method of Patankar [14] was used to the handle the pressure-velocity coupling. Fig. 2 presents a typical control volume written in the generalized coordinates system $\eta - \xi$. Although in the present work the computational domain of Fig. 1(b) is calculated using a Cartesian grid, Fig. 2 is here included indicating that the code employed was developed for generalized coordinates and appropriated to be used in any two-dimensional or axi-symmetric geometry. As such, the discretized form of the two-dimensional conservation equation for a generic property φ, in permanent regime, is given by:

$$I_e + I_w + I_n + I_s = S_\varphi \tag{25}$$

where I_e, I_w, I_n and I_s represent, respectively, the fluxes of φ in the faces east, west, north and south of the control volume and S_φ its source term.

Standard source term linearization is accomplished by using,

$$S_\varphi \approx S_\varphi^{**} \langle \varphi \rangle_P^i + S_\varphi^* \tag{26}$$

Discretization of the momentum equation in the x-direction gives,

$$S^{*x} = (S_e^{*x})_P - (S_w^{*x})_P + (S_n^{*x})_P - (S_s^{*x})_P + S_P^* \tag{27}$$

$$S^{**x} = S_\phi^{**} \tag{28}$$

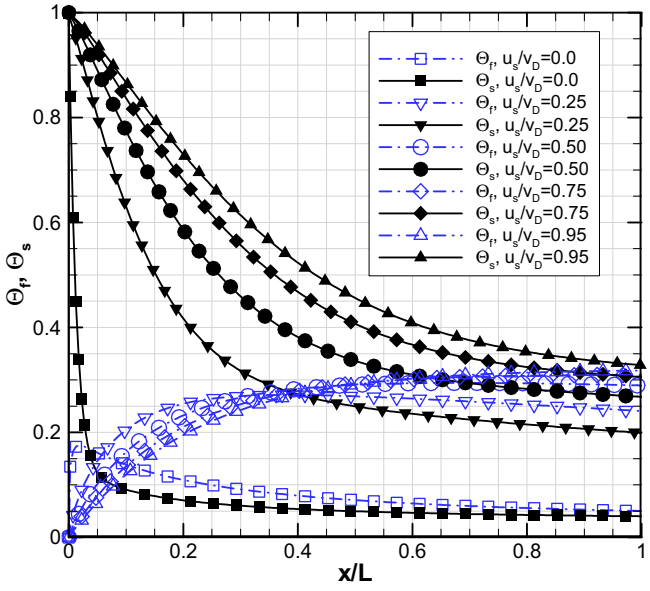

Fig. 6. Non-dimensional temperatures along the symmetry line $y = H$ as a function of u_s/v_D, $k_s/k_f = 25$, $\phi = 0.9$, $Re_D = 100$, $Da = 3.37 \times 10^{-3}$, $(\rho c_p)_s/(\rho c_p)_f = 1.5$.

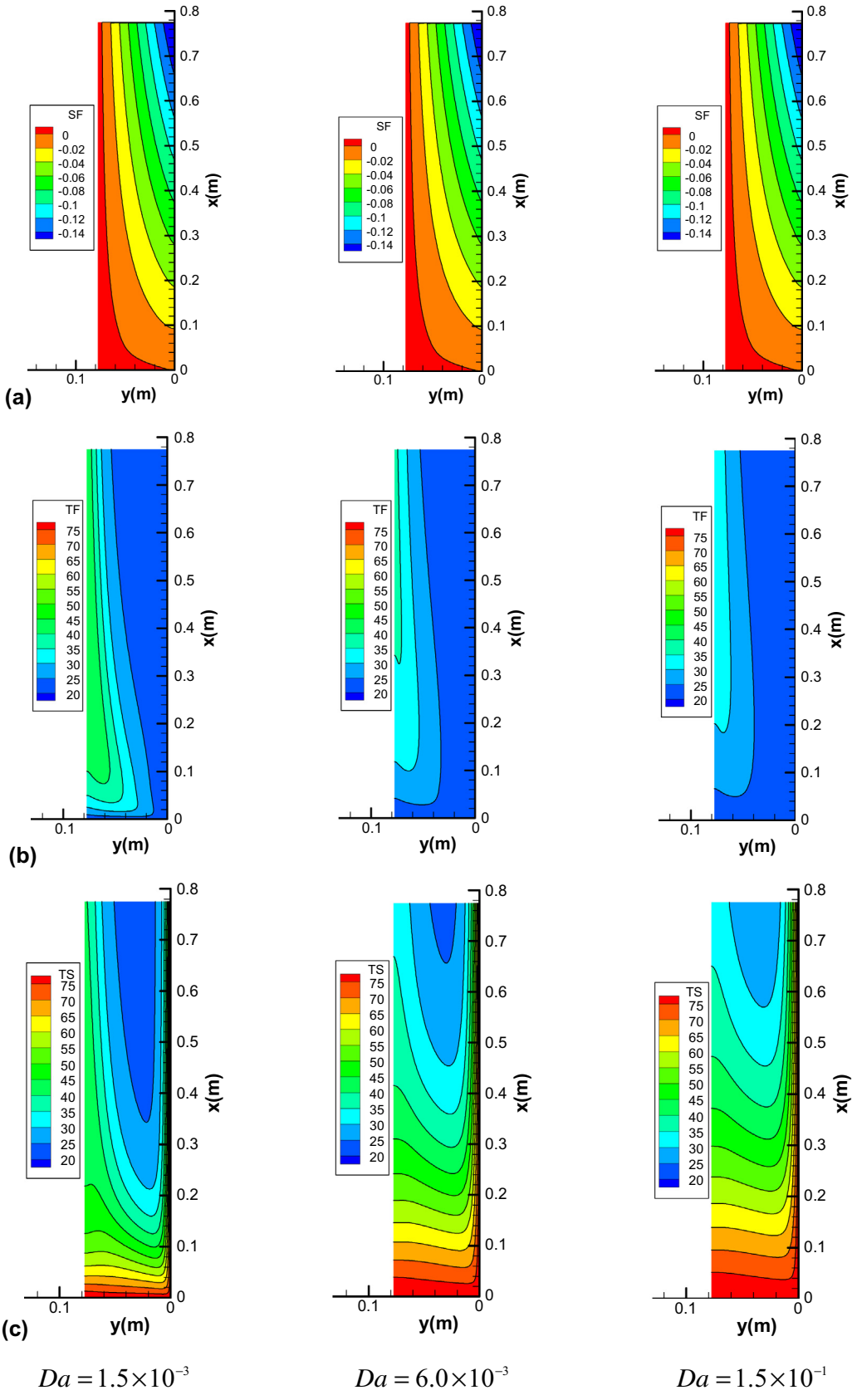

Fig. 7. Dimensional temperatures as a function of Da, $u_s/v_D = 0.5$, $\phi = 0.9$, $(\rho c_p)_s/(\rho c_p)_f = 1.5$, $k_s/k_f = 25$: (a) streamlines, (b) fluid temperature, (c) solid temperature.

where, S^{*x} is the diffusive part, here treated in an implicit form. The second term, S^{**x}, entails the additional drag forces due to the porous matrix, which are here treated explicitly.

Convergence was monitored in terms of the normalized residue, which was set to be lower than 10^{-9}.

2. Results and discussion

As mentioned above, the fluid and solid phases are given different temperatures at the inlet and non-dimensional temperatures for the solid and fluid are defined as:

$$\theta_{s,f} = \frac{\langle T_{s,f}\rangle^i - T_{\min}}{T_{\max} - T_{\min}} \tag{29}$$

where the subscripts s, f stands for the solid and fluid phases, respectively, and "max" and "min" refers to both temperature maximum and minimum of either phase. All cases run are compiled in Table 1 where dimensional and non-dimensional parameters are described.

Before presenting the results, a note on modeling validation seems timely. In Ref. [4], simulations using the laminar version of the mathematical model and numerical method here described were compared with analytical solutions by Nakayama and Kuwahara et al. As more data is gathered in the literature for turbulent regime, a more in-depth and complete validation procedure can be pursued. For the time being, however, comparisons with analytical solutions are expected to guarantee the correctness of the code developed and to reduce uncertainties on the results here presented.

2.1. Effect of Reynolds number, Re_D

The values used to vary Reynolds number Re_D, according to Table 1, were $Re_D = 10$, $Re_D = 50$ and $Re_D = 100$ where Re_D is defined by Eq. (20).

Fig. 3 shows two-dimensional maps for streamlines and temperature fields. Fig. 3(a) indicates that Reynolds variation affect strongly the flow behavior. This occurs due to mass flow increasing through the boundaries pushing the flow to the symmetry line increasing the velocity at the center of the reactor. Regarding the heat transfer between the phases, it is observed in Fig. 3(b) and (c) that there is a decrease of the temperature gradient at $x = 0$ with Reynolds number increasing. Also, the solid phase is better cooled as Re_D increases, as expected. As mentioned above, both the fluid and solid velocities are equal in the longitudinal direction, $u_D = u_s$, while the fluid velocity in the transversal direction, v_D, is increased for having a larger value for Re_D. Then, the component of the relative velocity in the longitudinal direction is null and in the transversal direction is v_D (see Fig. 3(c)). Fig. 4 shows values for longitudinal non-dimensional temperature profiles along the symmetry line of the channel, where it is noticed that for low Re_D the fluid temperatures attains higher values than Θ_s at the exit and along the centerline. When $v_{D_{in}}$ is increased, $Re_D = 100$, the equilibrium temperature is reached before the end of the reactor and the cooling effect of the solid phase is more pronounced. As such, as the solid moves faster in relation to the fluid, the stirring effect is stronger leading to enhancement of heat transfer between phases.

2.2. Effect of slip ratio, $\mathbf{u}_s/\mathbf{u}_D$

In Figs. 5 and 6 the effect of varying $\mathbf{u}_s/\mathbf{u}_D$ is evaluated while keeping fixed the transversal velocity v_D, or say, Re_D was fixed (see Fig. 1(c) and Eq. (20)) whereas the inlet mass flow at the west face, for both the solid and the fluid, were of equal value (see Table 1). Fig. 5(a) shows that increasing the west flow rate does not affect much the flow distribution, as far as the streamlines are considered. Further, one can examine the heat transfer between fluid and solid phases when u_s and u_D approaches to fluid velocity value in transversal direction, v_D. Fig. 5(b) and (c) shows that it takes longer for the solid to be cooled as u_s is increased. Also, as more energy is carried inside the reactor by convection, solid temperatures everywhere are higher for higher values of u_s. It is further noticed that when the slip ratio $\mathbf{u}_s/\mathbf{u}_D$ tends to 1, the heat transfer between the phases occurs manly by conduction so that the length necessary for thermal equilibrium is increased (Fig. 6).

2.3. Effect of Darcy number, Da

Another way to verify flow behavior and heat transfer between fluid and solid phases is through variation of the particle diameter D with consequent variation of permeability K, which is here calculated via the Ergun [15] equation,

$$K = D^2\phi^3/144(1-\phi)^2 \tag{30}$$

Eq. (30) gives the permeability K in terms of the particle diameter D and porosity ϕ and was proposed for packed beds. The Darcy number is then calculated as $Da = K/H^2$. As such, the porous beds here considered are composed of solid particles having size D. Depending on how spaced apart these particles are distributed within the medium, different porosities are obtained. Therefore, the use of Eq. (30) implies in assuming that the Darcy number Da, as well as the permeability K, are a function of both D and ϕ. In the results to be shown in this section on the effect of Da, the porosity is kept constant and equal to 0.9 whereas the particle diameter is varied giving the values for K compiled in Table 1.

Further, as mentioned, the problem under investigation here can be described as a heated solid matrix moving along the reactor being cooled by fluid stream flowing in both longitudinal and transverse directions. The variation of the particle diameter, keeping constant the porosity, will directly affect the permeability of the medium, where, the greater the particle diameter D, the greater will be the medium permeability K, as seen by the formulae above.

Fig. 7(a) indicates that the flow distribution is not much affected by the particle size, however, when the permeability of

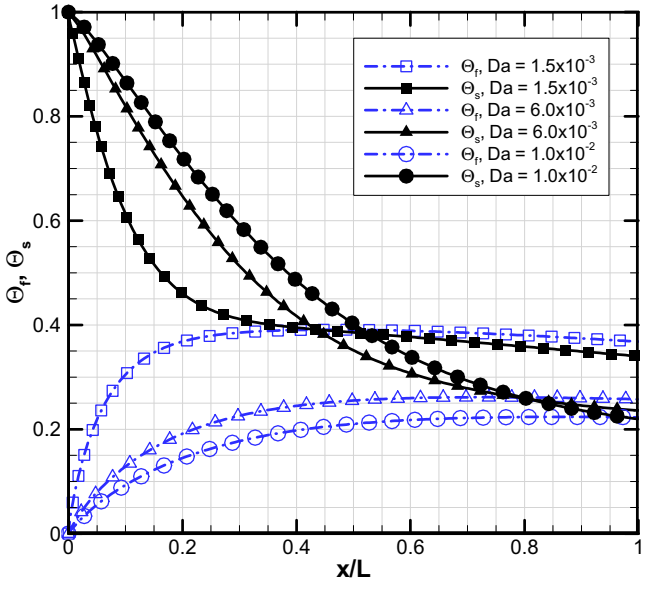

Fig. 8. Non-dimensional temperatures along the symmetry line $y = H$ as a function of Da, $u_s/v_D = 0.5$, $(\rho c_p)_s/(\rho c_p)_f = 1.5$, $k_s/k_f = 25$, $\phi = 0.9$.

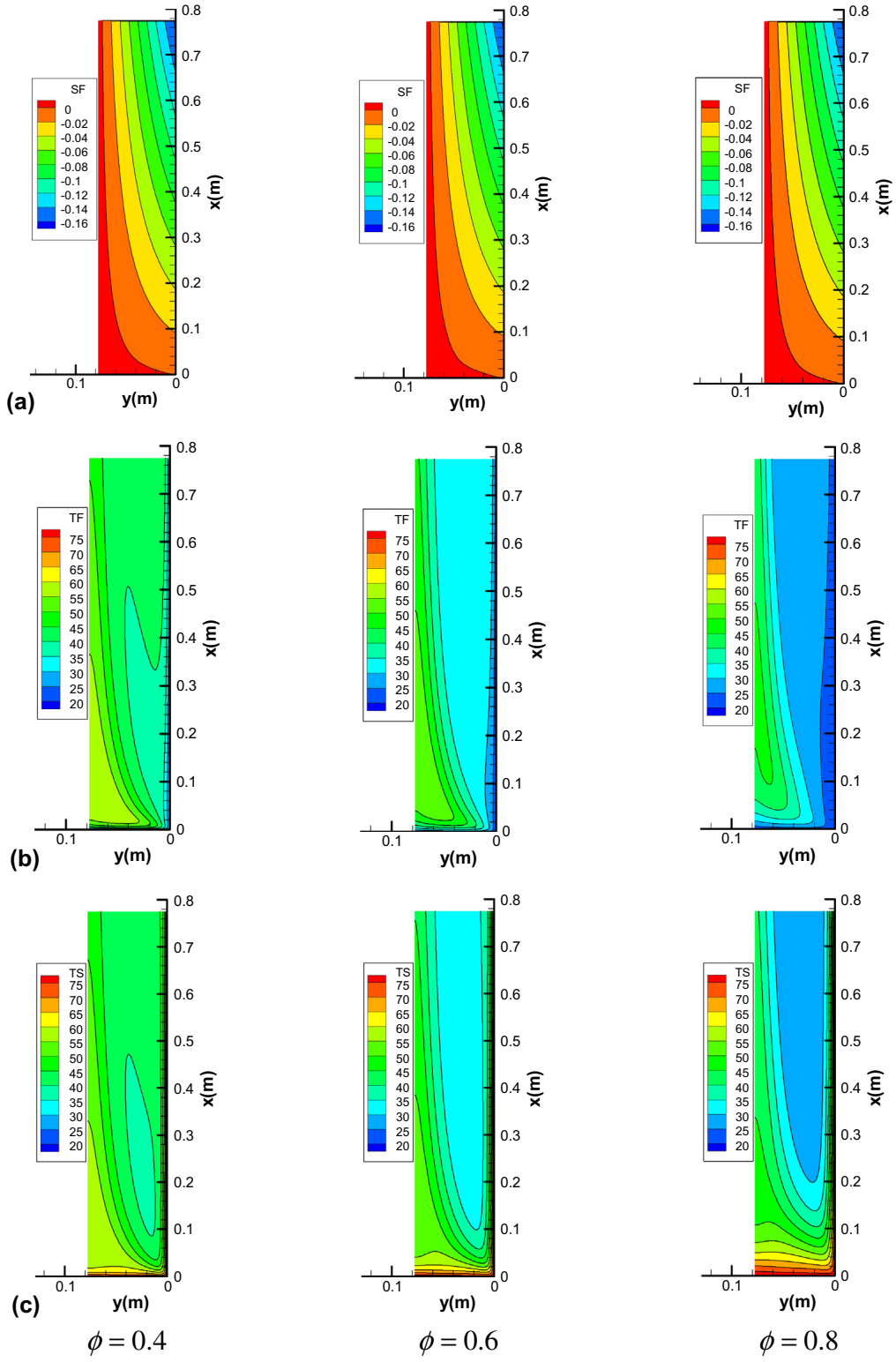

Fig. 9. Dimensional temperatures as a function of ϕ, $u_s/v_D = 0.5$, $(\rho c_p)_s/(\rho c_p)_f = 1.5$, $Re_D = 75$, $k_s/k_f = 25$: (a) streamlines, (b) fluid temperature, (c) solid temperature.

the medium is reduced by decreasing D, a larger interfacial area is obtained and a quicker heat transfer rate between the two phases is achieved. This effect can be seen by inspecting Fig. 7(b) and (c). This effect is further presented when inspecting Fig. 8 that shows the behavior of both temperatures at the centerline of the reactor. For higher values of Da, or say, for higher particle diameter D, less interfacial area impacts on interfacial heat transfer rates and bring the equilibrium temperature to a lower value at the reactor exit. Or say, the fluid is not heated up as much as in the case of a larger interfacial area (lower Da).

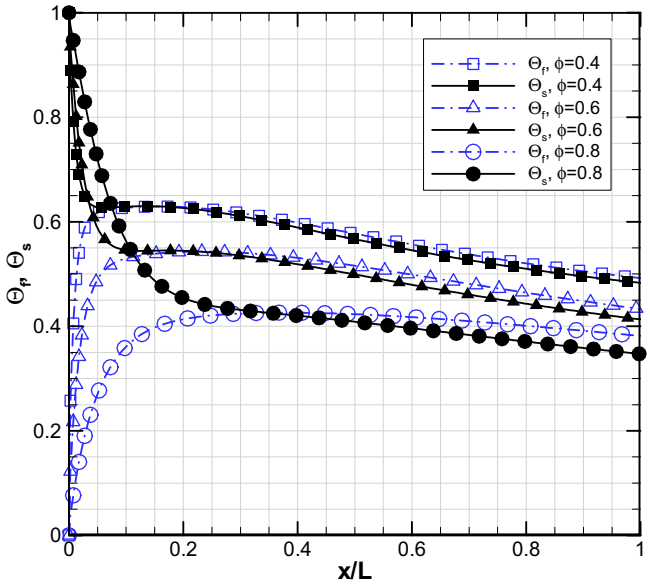

Fig. 10. Non-dimensional temperatures along the symmetry line $y = H$ as a function of ϕ, $u_s/v_D = 0.5$, $(\rho c_p)_s/(\rho c_p)_f = 1.5$, $Re_D = 75$, $k_s/k_f = 25$, $Re_D = 100$.

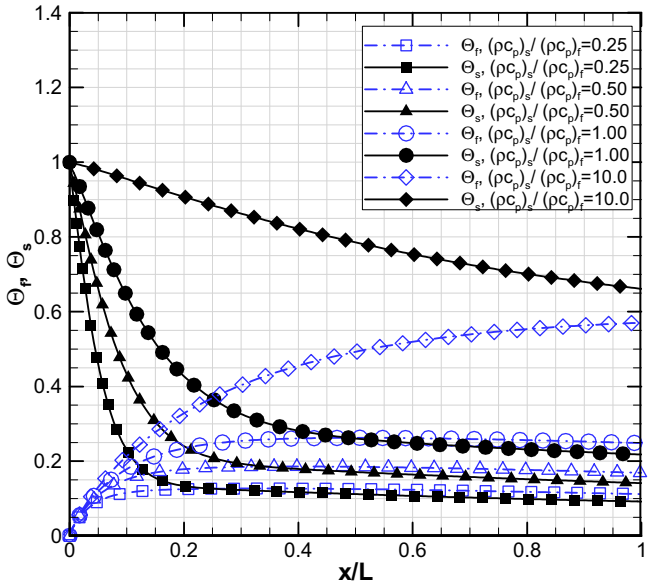

Fig. 12. Non-dimensional temperatures along the symmetry line $y = H$ as a function of $(\rho c_p)_s/(\rho c_p)_f$, $u_s/v_D = 0.5$, $k_s/k_f = 25$, $\phi = 0.9$, $Da = 3.37 \times 10^{-3}$, $Re_D = 75$.

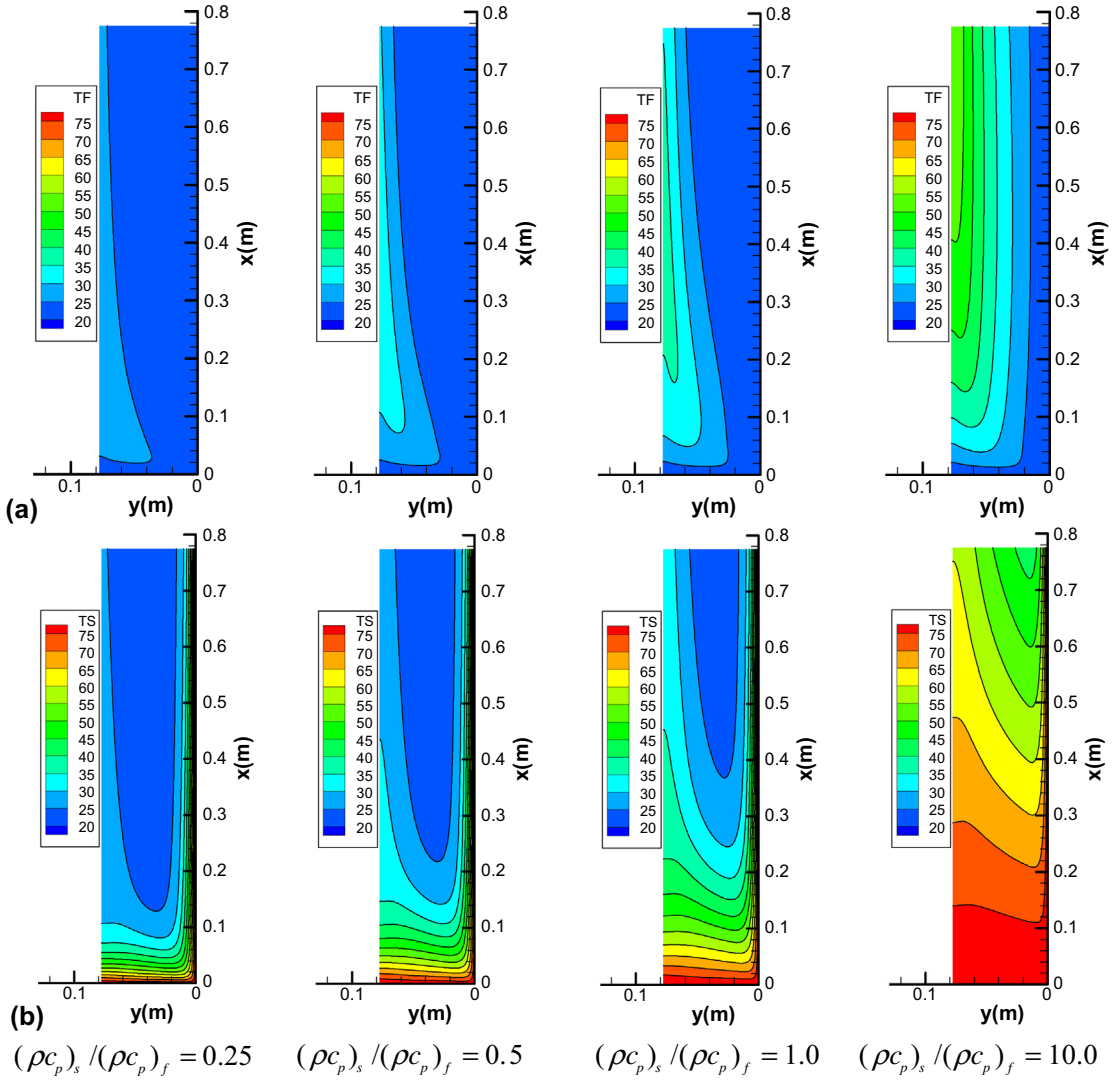

Fig. 11. Dimensional temperatures as a function of $(\rho c_p)_s/(\rho c_p)_f$, $Re_D = 75$, $u_s/v_D = 0.5$, $k_s/k_f = 25$, $\phi = 0.9$, $Da = 3.37 \times 10^{-3}$: (a) fluid temperature, (b) solid temperature.

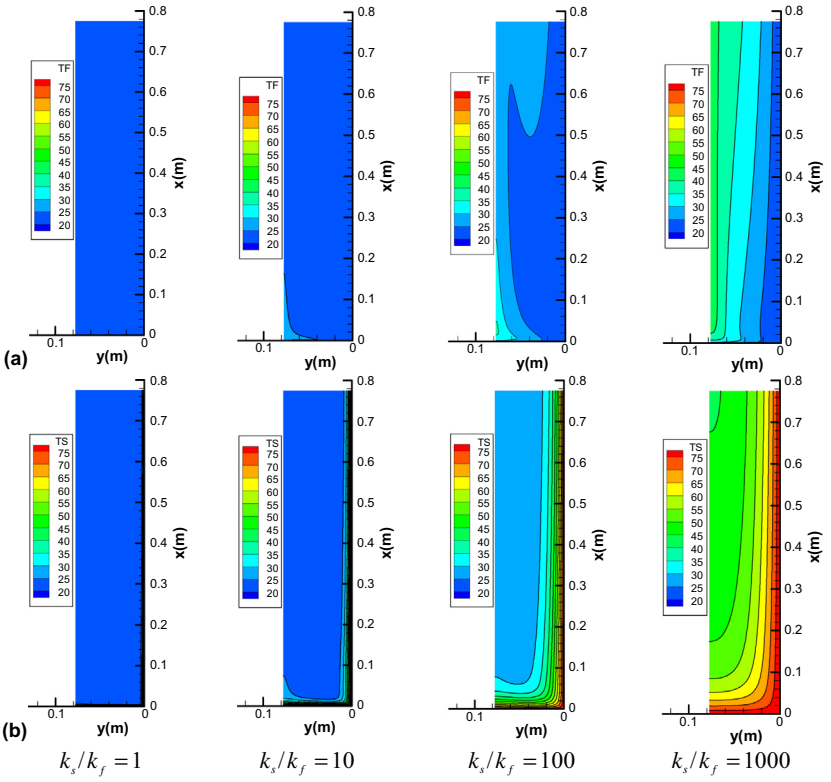

Fig. 13. Dimensional temperatures as a function of k_s/k_f, $\phi = 0.9$, $Re_D = 75$, $u_s/v_D = 0$, $Da = 3.37 \times 10^{-3}$, $(\rho c_p)_s/(\rho c_p)_f = 1.5$: (a) fluid temperature, (b) solid temperature.

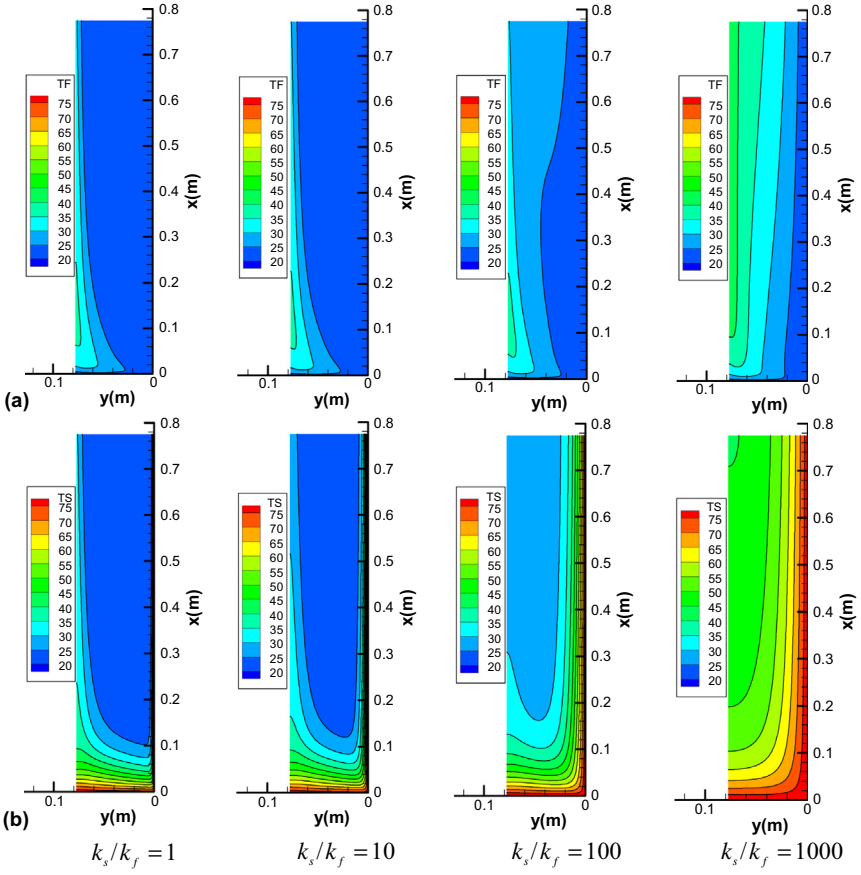

Fig. 14. Dimensional temperatures as a function of k_s/k_f, $Re_D = 75$, $Da = 3.37 \times 10^{-3}$, $(\rho c_p)_s/(\rho c_p)_f = 1.5$, $u_s/v_D = 0.1$, $\phi = 0.9$: (a) fluid temperature, (b) solid temperature.

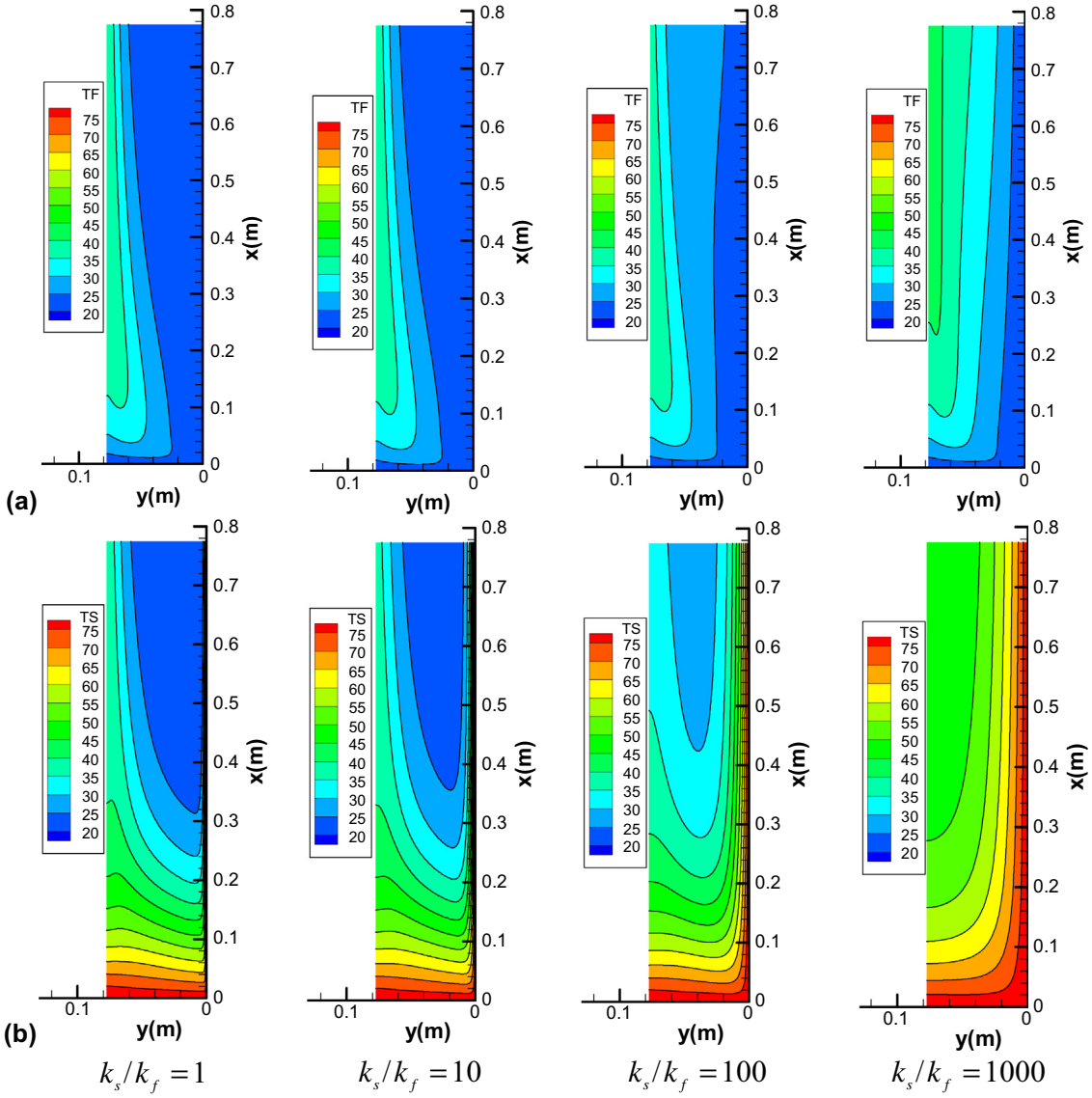

Fig. 15. Dimensional temperatures as a function of k_s/k_f, $Re_D = 75$, $Da = 3.37 \times 10^{-3}$, $(\rho c_p)_s/(\rho c_p)_f = 1.5$, $u_s/v_D = 0.4$, $\phi = 0.9$: (a) fluid temperature, (b) solid temperature.

2.4. Effect of porosity, ϕ

Porosity effect upon bidimensional flow and heat transfer for a crossflow moving bed is further shown in Fig. 9. Again it can be seen in Fig. 9(a) that the flow distribution is not much affected by changing porosity. The values of the porosity used in this simulation were 0.4, 0.6 and 0.8. Here, it is important to mention that although in for granular beds porosities are in general below 0.6, the model here considered was developed for porous media having sufficient void space for turbulence to be developed within the pores [8]. Therefore, although here only laminar flow is investigated, simulation of turbulence in highly porous media is the final goal of this systematic work. Further, it is also emphasized that the treatment of the solid phase is such that a unique velocity is assumed for the entire porous matrix, which reflects practical situations more related to packed moving beds, as in gasifiers, than the movement of dispersed granular material, as in fluidized bed systems.

The longitudinal temperature field for the transversal solid-fluid is shown in Fig. 9(b) and (c). It is observed that with the increasing of the porosity there is a decrease in the temperature gradient for both fluid and solid phases at the west inlet. Also, as ϕ increases, a deeper cooling of the porous material is obtained, reflecting the fact that the cooling fluid penetrates more easily into the core of the layer as the void space becomes larger size. It can also be seen in Fig. 10 that the effect of the porosity on the longitudinal temperature distribution along the symmetry line is to elongate the length for thermal equilibrium as ϕ increases. On the other hand, for small porosity a quicker thermal equilibrium is reached at expense of increasing the equilibrium temperature at the exit.

2.5. Effect of thermal capacity ratio, $(\rho c_p)_s/(\rho c_p)_f$

In this simulation, the fluid thermal capacity $(\rho c_p)_f$ was kept constant whereas the solid thermal capacity $(\rho c_p)_s$ was increased. Here, the streamlines are not shown because the same velocity distribution was considered in all cases. Through Fig. 11(a) and Fig. 11(b) it is noticed that the increasing the specific heat of the solid material causes an increasing in the fluid temperature as more energy per unit mass is brought into the

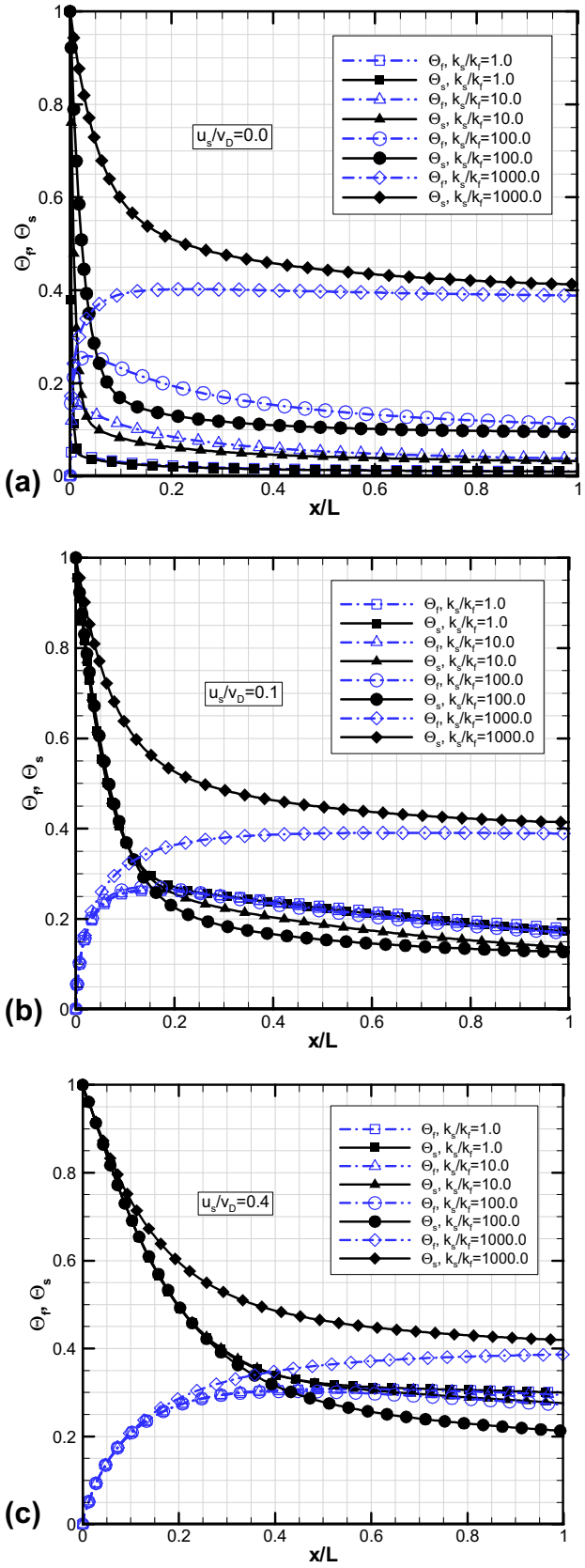

Fig. 16. Non-dimensional temperatures along the symmetry line $y = H$ as a function of k_s/k_f for $Re_D = 75$, $\phi = 0.9$, $Da = 3.37 \times 10^{-3}$, $(\rho c_p)_s/(\rho c_p)_f = 1.5$: (a) $u_s/v_d = 0.0$, (b) $u_s/v_D = 0.1$, (c) $u_s/v_D = 0.4$.

system. Temperature gradients at west inlet are also decreased and overall temperatures of both phases raises as $(\rho c_p)_s/(\rho c_p)_f$ increases. These results can be better observed in noting the temperature behavior along the symmetry line in Fig. 12. For a higher ratio $(\rho c_p)_s/(\rho c_p)_f$ the solid temperature keeps is high value, heating up the fluid and leading to a higher fluid temperature at the east exit.

2.6. Effect of thermal conductivity ratio, k_s/k_f

For this set of simulations, the fluid thermal conductivity k_f was kept constant, varying only the solid thermal conductivity k_s. As in the case of the ratio $(\rho c_p)_s/(\rho c_p)_f$, the effect of the variable analyzed here, namely k_s, did not influence the flow behavior at all and for that no streamlines pattern are presented below. Below, three values for the ratio u_s/v_D was chosen, namely 0.0, 0.1 and 0.4.

When solid is not moving, Fig. 13, an increasing in the value of the thermal conductivity of the solid causes an increase in the solid temperature by conduction along the longitudinal axis of the reactor. That can be seen in Fig. 13(a) and (b). Further, with the movement of the solid phase for other two cases, *i.e.*, $u_s/v_D = 0.1$ (Fig. 14) and $u_s/v_D = 0.4$ (Fig. 15), while keeping constant the fluid velocity in the transversal direction v_D, all temperature tend to rise due to the increase of the thermal conductivity throughout the equipment. At the exit, fluid temperature will be higher due to the fact that solid temperatures are also higher due to the elevated solid thermal temperatures. This effect is more evident if one compares the behavior of both temperatures for the three solid phase velocities shown in Fig. 16. So, for moving bed cases, there is an improvement on the heat transfer rate from the solid to the fluid when temperatures for the fixed bed (Fig. 16(a)) are compared to those considering a moving solid structure (Fig. 16(b) and (c)).

3. Conclusions

This work investigated the effect thermal property variation on the flow behavior and heat transfer between fluid and solid phases for longitudinal and transversal flow using the two energy equation with the thermal non-equilibrium model.

In summary, for a larger interfacial area, obtained by either decreasing *Da* or porosity, both phases attain the equilibrium temperature within a shorter developing length. For the three cases of thermal conductivity ratio here analyzed, it is seen that for high k_s/k_f cases, temperature gradients for both fluid and solid phases decreases since a higher solid thermal conductivity transport heat more easily through the solid, which, in turn, heats up the fluid via interfacial heat transfer.

In all simulations, the fluid temperature reaches its highest values in the symmetry plane of the channel. This occurs mainly for high values of the u_s/u_D, $(\rho c_p)_s/(\rho c_p)_f$ and k_s/k_f, where, in these cases, both fluid and solid temperatures rise due the high values of these parameters. For high values of Re_D, *Da* and ϕ, the fluid temperature decreases along the channel, mainly in the symmetry line.

Acknowledgments

The authors are thankful to FAPESP and CNPq, Brazil, for their invaluable financial support during the course of this research.

References

[1] J. Zhao, J. Huang, J. Wu, Y. Fang, Y. Wang, Modeling and optimization of the moving granular bed for combined hot gas desulfurization and dust removal, Powder Technol. 180 (2008) 2–8.

[2] A. Lozano, V. Henriquez, A.M. Machin, Modeling of a new crossflow moving-bed heat-exchanger filter, Filtr. Sep. (1996) 69–74.

[3] J.A. Almendros-Ibáñez, A. Soria-Verdugo, U. Ruiz-Rivas, D. Santana, Solid conduction effects and design criteria in moving bed heat exchangers, Appl. Therm. Eng. 31 (2011) 1200–1207.

[4] A.C. Pivem, M.J.S. de Lemos, Laminar heat transfer in a moving porous bed reactor simulated with a macroscopic two-energy equation model, Int. J. Heat Mass Transfer 55 (7–8) (2012) 1922–1930.

[5] A.C. Pivem, M.J.S. de Lemos, Temperature distribution in a counterflow moving bed under a thermal nonequilibrium condition, Numer. Heat Transfer 61 (2012) 1–17.

[6] M.B. Saito, M.J.S. de Lemos, Interfacial heat transfer coefficient for non-equilibrium convective transport in porous media, Int. Commun. Heat Mass Transfer 32 (5) (2005) 666–676.

[7] M.J.S. de Lemos, M.B. Saito, Computation of turbulent heat transfer in a moving porous bed using a macroscopic two-energy equation model, Int. Commun. Heat Mass Transfer 35 (2008) 1262–1266.

[8] M.J.S. de Lemos, Turbulence in Porous Media: Modeling and Applications, second ed., Elsevier, Amsterdam, 2012.

[9] W.G. Gray, P.C.Y. Lee, On the theorems for local volume averaging of multiphase system, Int. J. Multiphase Flow 3 (1977) 333–340.

[10] S. Whitaker, Advances in theory of fluid motion in porous media, Ind. Eng. Chem. 61 (1969) 14–28.

[11] M.B. Saito, M.J.S. de Lemos, A correlation for interfacial heat transfer coefficient for turbulent flow over an array of square rods, J. Heat transfer 128 (2006) 444–452.

[12] N. Wakao, S. Kaguei, T. Funazkri, Effect of fluid dispersion coefficients on particle–fluid heat transfer coefficient in packed bed, Chem. Eng. Sci. 34 (1979) 325–336.

[13] F. Kuwahara, M. Shirota, A. Nakayama, A numerical study of interfacial convective heat transfer coefficient in two-energy equation model for convection in porous media, Int. J. Heat Mass Transfer 44 (2001) 1153–1159.

[14] S.V. Patankar, Numerical Heat Transfer and Fluid Flow, Hemisphere, Washington, DC, 1980.

[15] S. Ergun, Fluid flow through packed columns, Chem. Eng. Prog. 48 (1952) 89–94.